Water Research 267 (2024) 122548

Contents lists available at ScienceDirect

Water Research

journal homepage: www.elsevier.com/locate/watres

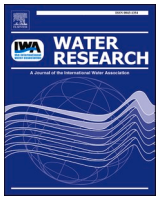

Cysteine-Facilitated Cr(VI) reduction by Fe(II/III)-bearing phyllosilicates: Enhancement from *In-Situ* Fe(II) generation

Fei Wu [a], Jing Sun [a], Fangyuan Meng [a], Jimei Zhou [b], Meng Qi [a], Xiaoli Lu [a], Chengshuai Liu [a,c,*]

[a] State Key Laboratory of Environmental Geochemistry, Institute of Geochemistry, Chinese Academy of Sciences, Guiyang 550081, China
[b] The key Laboratory of Environmental Pollution Monitoring and Disease Control, Ministry of Education & School of Public Health, Guizhou Medical University, Guiyang 550025, China
[c] College of Natural Resources and Environment, South China Agricultural University, Guangzhou, 510650, China

ARTICLE INFO

Keywords:
Fe-bearing phyllosilicates
Electron shuttle
Interfacial electron transfer
In-situ produced Fe(II), Cr(VI) reduction

ABSTRACT

Structural Fe in phyllosilicates represents a crucial and potentially renewable reservoir of electron equivalents for contaminants reduction in aquatic and soil systems. However, it remains unclear how *in-situ* modification of Fe redox states within Fe-bearing phyllosilicates, induced by electron shuttles such as naturally occurring organics, influences the fate of contaminants. Herein, this study investigated the processes and mechanism of Cr(VI) reduction on two typical Fe(II/III)-bearing phyllosilicates, biotite and chlorite, in the presence of cysteine (Cys) at circumneutral pH. The experimental results demonstrated that Cys markedly enhanced the rate and extent of Cr(VI) reduction by biotite/chlorite, likely because of the formation of Cr(V)-organic complexes and consequent electron transfer from Cys to Cr(V). The concomitant production of non-structural Fe(II) (including aqueous Fe (II), surface bound Fe(II), and Cys-Fe(II) complex) cascaded transferring electrons from Cys to surface Fe(III), which further contributed to Cr(VI) reduction. Notably, structural Fe(II) in phyllosilicates also facilitated Cr(VI) reduction by mediating electron transfer from Cys to structural Fe(III) and then to edge-sorbed Cr(VI). ^{57}Fe Mössbauer analysis revealed that *cis*-coordinated Fe(II) in biotite and chlorite exhibits higher reductivity compared to *trans*-coordinated Fe(II). The Cr end-products were insoluble Cr(III)-organic complex and sub-nanometer Cr_2O_3/$Cr(OH)_3$, associated with residual minerals as micro-aggregates. These findings highlight the significance of *in-situ* produced Fe(II) from Fe(II/III)-bearing phyllosilicates in the cycling of redox-sensitive contaminants in the environment.

1. Introduction

The prevalence, reactivity, swelling property, and environmental compatibility of Fe-bearing minerals have made them integral to biogeochemical processes, including the adsorption, oxidation, and reduction of contaminants in terrestrial and aquatic environments (Dong, 2012; Fan et al., 2023; Huang et al., 2021; Jaisi et al., 2009; Kantar et al., 2015; Liu et al.,2023). Structural Fe in phyllosilicates contributes significantly to the total Fe mass in the environment (Favre et al., 2006; Luan et al., 2015). The Fe(III) bound within the structure of phyllosilicates can potentially undergo reduction through chemical or microbial mechanisms (Deng et al., 2023; Morrison et al., 2013; Neumann et al., 2013; Luan et al., 2015). The resulting structural Fe(II) is capable of serving as an electron donor and subsequently reducing various redox-sensitive contaminants, such as Cr(VI), U(VI), nitrobenzene, and tetracyclines (Chen et al., 2019; Joe-Wong et al., 2017; Luan et al., 2015; Satpathy et al., 2022; Zhang et al., 2022). Previous studies utilizing ^{57}Fe Mössbauer spectrum indicated that multiple types of Fe(II) sites are present in phyllosilicates (Brookshaw et al., 2014a, b; De Grave et al., 1987; He et al., 2005). However, how the structural variations of these Fe(II) entities regulate their reactivities and the mechanisms of electron transfer from phyllosilicates to contaminants remains poorly understood.

Due to the layered structure of phyllosilicates, Fe(II) is primarily confined within the octahedral sheets of Fe(II/III)-bearing phyllosilicates. Consequently, the reduction of contaminants by structural Fe(II) involves electron transfer from the inner lattice to the outer surface of phyllosilicates (Bishop et al., 2019; Joe-Wong et al., 2017; Liao et al., 2019; Zhang and Jun, 2018). The reduction capacity and kinetics are influenced by various factors, including the intrinsic properties of

* Corresponding author at: 99 Lincheng West Road, Guanshanhu District, Guiyang 550081, P R China.
E-mail address: liuchengshuai@vip.gyig.ac.cn (C. Liu).

https://doi.org/10.1016/j.watres.2024.122548
Received 17 June 2024; Received in revised form 17 September 2024; Accepted 28 September 2024
Available online 29 September 2024

phyllosilicates (e.g., structure and Fe(II) content), experimental conditions (e.g., pH and ionic strength), and other environmental factors (e.g., microbes and organics) (Bishop et al., 2019, 2014; Brookshaw et al., 2014a; Joe-Wong et al., 2017; Zhang et al., 2022). In particular, organics often coexist with phyllosilicates in natural systems, significantly impacting their reduction capacity (Deng et al., 2023; Liu et al., 2018; Zhang et al., 2021). For instance, citrate and ethylenediaminetetraacetic acid (EDTA) can enhance U(VI) bioreduction in the presence of nontronite because soluble Fe(III)- and Fe(II)-citrate/EDTA complexes can act as electron shuttles to expedite U(VI) bioreduction (Zhang et al., 2021). However, Suwannee River natural organic matter and citrate have been reported to inhibit Cr(VI) reduction by competing with Cr(VI) for adsorption sites on the surface of reduced nontronite (Deng et al., 2023; Liu et al., 2018).

Previous studies on the reduction of contaminants by Fe(II/III)-bearing phyllosilicates often used chemically or biologically pre-reduced mineral specimens (Bishop et al., 2014; Brookshaw et al., 2014a; Joe-Wong et al., 2017). In natural environments, the co-existence of phyllosilicates, microorganisms and/or organics can lead to the *in-situ* formation of both structural and non-structural Fe(II) (Brookshaw et al., 2014b; Deng et al., 2023; Fang et al., 2023; Luan et al., 2015; Morrison et al., 2013). This *in-situ* produced Fe(II) can facilitate redox-active contaminants reduction, such as carcinogenic Cr (VI). Cr(VI) is among the most toxic elements and is considered a priority pollutant in groundwater and soils, with its toxicity and mobility closely linked to the structural evolution of Fe-bearing minerals (Brookshaw et al., 2014a; Liao et al., 2019). Moreover, many naturally occurring organics, such as cysteine (Cys) and desferrioxamine B (DFOB), can also reduce Cr(VI) (Lay and Levina, 1996; Liu et al., 2022; Morrison et al., 2013). However, it remains unclear whether and how these organics influence the kinetics and mechanism of Cr(VI) reduction by Fe (II/III)-bearing phyllosilicates. In such systems, structural Fe(III) reduction may compete with Cr(VI) reduction for available electron donors, and/or produce Fe(II) *in-situ* that serves as an additional reductant for Cr(VI) (Kim et al., 2019; Wang et al., 2019; Wielinga et al., 2001).

An increasing body of evidence proves that various organic molecules serve as electron shuttles, significantly impacting on Fe biogeochemical cycles, mineral structure evolution, and pollutant transformation (Doong and Schink, 2002; Fang et al., 2023; Hu et al., 2021; Liu et al., 2018; Morrison et al., 2013). For instance, small organic molecules such as lignin and Cys could act as electron shuttles to transfer electrons to the surface and structural of Fe-bearing minerals (Doong and Schink, 2002; Morrison et al., 2013; Sheng et al., 2021). Of these electron shuttles, Cys is commonly found in terrestrial and aquatic environments due to the metabolism and decay of organisms (Hu et al., 2021; Morrison et al., 2013). With a notably low reduction potential ($E_H = -348$ mV) (Jocelyn, 1967), Cys can effectively reduce structural Fe (III) in Fe(III) oxides and Fe(III) phyllosilicates (Doong and Schink, 2002; Li et al., 2022; Morrison et al., 2013; Sun et al., 2020), thereby enhancing their reducing capacity. Meanwhile, Cys could adsorb/intercalate into the interlayer spaces of 2:1 type phyllosilicates, which may alter the reactivity of structural Fe(II) toward pollutants (De Santana et al., 2010; Morrison et al., 2013). Although the impact of Cys on the structural evolution of phyllosilicates have been recognized, little is known about the alterations in electron transfer interfacial processes between Fe(II/III)-phyllosilicates and pollutants after their interactions with Cys. The current knowledge limited to the *in-situ* produced Fe(II) may underestimate the transformation of pollutants in conjunction with the Fe biogeochemical cycling (Sun et al., 2020; Wang et al., 2019).

The objectives of this study were therefore (i) to assess the capability of Cys as a potential electron carrier for inducing the reductive transformation of Fe(II/III)-bearing phyllosilicates, and its influence on the dynamics and mechanisms of Cr(VI) reduction, (ii) to identify potential variations in the reactivity of Fe(II) at various structural sites within phyllosilicates during electron transfer, and (iii) to examine the associated influence on Cr speciation and distribution. A series of Cr(VI) reduction experiments in which Cys and phyllosilicates were added simultaneously or separately were conducted and compared. Biotite and chlorite, two common Fe(II/III)-bearing phyllosilicates, were selected due to their likely representation of a significant percentage of the reducible Fe(III) in terrestrial soils as well as marine and lake sediments (Brookshaw et al., 2015). The *in-situ* Fe(II) generation, Cr distribution, and mineralogical variation were concurrently measured. Our data provides valuable insights into the interfacial electron transfer of redox-active pollutants on Fe-bearing phyllosilicates in aquatic and terrestrial ecosystems, and has substantial implications for the development of a long-term, *in-situ* immobilization technology for Cr(VI) remediation.

2. Materials and methods

2.1. Chemicals

Biotite used in the experiments was acquired from Shanghai Macklin Biochemical Co., Ltd, with a particle size of approximately 38 μm. Chlorite was obtained from Youyan (Liaoning, China) and sieved to < 74 μm. Based on powder X-ray diffraction (XRD), the biotite was monomineralic and the chlorite was identified to be clinochlore (Figure S1). X-ray fluorescence (XRF) analysis and ^{57}Fe Mössbauer revealed that the biotite contained 10.2 wt % Fe with 74.3 % Fe(II) and chlorite contained 9.9 wt % Fe with 89.8 % Fe(II) (Fig. 4, Table S1 and Table S3). The Brunauer Emmett Teller (BET) surface area of biotite and chlorite was 7.18 $m^2 \cdot g^{-1}$ and 3.11 $m^2 \cdot g^{-1}$, respectively.

L-cysteine ($HSCH_2CH(NH_2)CO_2H$, 97 % pure) was purchased from Sigma-Aldrich. Potassium dichromate ($K_2Cr_2O_7$), 5,5′-Dithiobis-(2-nitrobenzoic acid) (DTNB), and 2-(N-morpholino)-ethanesulfonic acid (MES) were obtained from Shanghai Macklin Biochemical Co., Ltd., China. All glassware was soaked in 5 % HNO_3 and washed three times with deionized water before use. All solutions were prepared with Milli-Q water (18.2 MΩ, Millipore, Merck).

2.2. Batch experiments and sampling

A series of Cr(VI) reduction experiments were performed in 150 mL serum vials at room temperature in an anaerobic glove box (Coy Laboratory Products, Grass Lake, MI, USA), with an atmosphere consisting of 96 % N_2 and 4 % H_2. A 10 mM KCl solution, buffered to a pH of 6.0 ± 0.05 with 10 mM MES (*pK*a 6.06) buffer, was employed as the background electrolyte. The chosen pH value aimed to mimic the slightly acidic to neutral pH range typically found in natural environments (Slessarev et al., 2016), while also minimizing phyllosilicates dissolution (Joe-Wong et al., 2017). The Si release of glass beaker was weak at the pH 6.0 and 25 °C (Bohrer et al., 2008), justifying their use as reaction vessels.

To investigate the combined effects of Cys and biotite/chlorite on Cr (VI) reduction, a ternary system [i.e., Cys + biotite/chlorite + Cr(VI)] was employed. 0.5 g biotite/chlorite was added to 100 mL of 10 mM MES buffer, and the suspension was equilibrated by stirring for 30 min. Subsequently, an appropriate amount of Cys was pre-mixed into the suspension, followed by the addition of a Cr(VI) stock solution to initiate the reduction process (Liu et al., 2019). The initial concentrations of both Cys and Cr(VI) were set at 0.5 mM. The relatively high concentrations of Cr(VI) and Cys were chosen to facilitate the mechanistic investigation and to characterize the Cr(III) end-products and structural changes of phyllosilicates (Liu et al., 2018, 2022; Morrison et al., 2013; Zhang et al., 2022). For the observation of the Cr(VI) reduction intermediate, specifically Cr(V), the concentrations of both Cys and Cr(VI) were adjusted to 5.0 mM in order to generate a sufficient amount of Cr (V) that could be readily detected using electron paramagnetic resonance spectroscopy (EPR). Although these higher concentrations might alter the kinetics of Cr(VI) reduction and Cr(V) formation compared to

lower concentrations, the fundamental mechanisms of Cr(VI) reduction and Cr(V) generation are expected to remain similar (Liu et al., 2019). Three binary control groups, specifically Cys + Cr(VI) and biotite/chlorite + Cr(VI), were established to assess the individual contributions of Cys or biotite/chlorite to Cr(VI) reduction. Two additional binary group of Cys + biotite/chlorite was conducted to investigate the intercalation of Cys with biotite/chlorite and the reduction of structural Fe(III) by Cys. All experiments were performed in duplicate. To prevent photo-oxidation, all reaction vials were covered with aluminum foil.

The total duration of the experiments was 10 days. At preselected time points, 0.8 mL of suspension was withdrawn and filtered through a 0.22 μm membrane (Jinteng, China) for analysis of aqueous Cr(VI) and aqueous total Cr. For experimental groups containing both phyllosilicates and Cys, the concentrations of aqueous Fe, Mg, and Si at the end of the reaction were determined to monitor the dissolution of minerals induced by Cys. After 5 days of reaction, a portion of the suspension was centrifuged under 12,000 g for 10 min. The solid-phase sample was collected, washed three times with deionized water, dried, and stored in the anaerobic glovebox before solid-phase characterization.

2.3. Analytical procedures

The concentration of aqueous Cr(VI) was determined using the 1,5-diphenylcarbazide (DPC) colorimetric assay (Liao et al., 2020). The total aqueous Cr concentration and the concentrations of aqueous Fe, Mg, and Si were monitored using inductively coupled plasma optical emission spectroscopy (ICP-OES, Agilent 700 Series, USA). Cys concentration was measured using the DTNB method (Ellman's reagent) (Text S1, Sun et al., 2020).

The phyllosilicates were characterized via XRD, Mössbauer spectroscopy, X-ray photoelectron spectroscopy (XPS), transmission electron microscopy (TEM), and EPR. Detailed information on the characterizations of samples is presented in Text S2.

3. Results and discussion

3.1. Cr(VI) reduction in the presence of both CYS and phyllosilicates

The reduction of Cr(VI) by Cys followed a typical kinetic process with an initial rapid decrease within the first 6 h, and then reached equilibrium in 24 h with a small increment (Figure S2a). The rate and extent of Cr(VI) reduction increased with the concentration of Cys, indicating the efficient degradation ability of Cys towards Cr(VI) (Cakir and Bicer, 2005; Lay and Levina, 1996). A small amount of Cr(VI) was removed over 10 days in the presence of phyllosilicates (5 $g{\cdot}L^{-1}$) alone (Fig. 1a, b), indicated that biotite and chlorite were not able to efficiently reduce Cr(VI) at the concentration studied, consistent with previous reports (Bishop et al., 2014; Brookshaw et al., 2014a; He et al., 2005). The low Cr(VI) removal can be ascribed to the fact that the negatively charged surface of biotite and chlorite at pH 6.0 becomes quite strong considering their point of zero below 4.5 (Luo et al., 2022; Zhou et al., 2020).

In comparison to individual treatments with biotite or chlorite, the Cr(VI) removal efficiency in the ternary systems [i.e., Cys + biotite/chlorite + Cr(VI)] significantly increased from 8.2 % and 12.0 % to 62.4

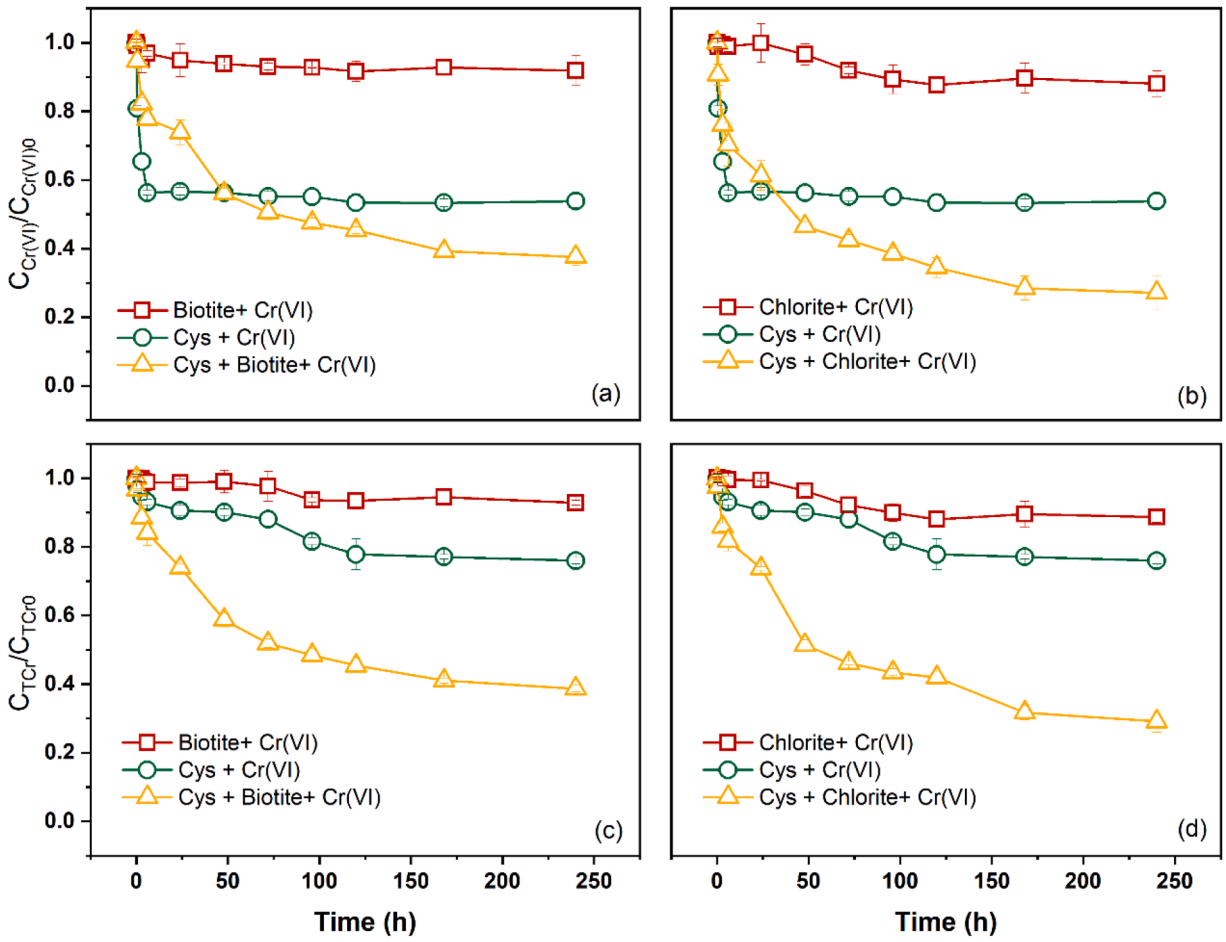

Fig. 1. The changes of aqueous Cr(VI) concentration ($C_{Cr(VI)}$) in the presence of (a) Cys + biotite, and (b) Cys + chlorite, and the total aqueous Cr concentration (C_{TCr}) of (c) Cys + biotite and (d) Cys + chlorite. Reaction conditions: 0.5 mM initial Cys, 0.5 mM initial aqueous Cr(VI), 5 $g{\cdot}L^{-1}$ biotite/ chlorite, and 10 mM KBr (pH 6.0 was buffered with MES). Error bars represent standard deviations from duplicate experiments, and some bars are smaller than the size of symbols.

% and 72.9 % after 10 days. However, relative to treatment with Cys alone, the combined presence of Cys and phyllosilicates initially suppressed Cr(VI) removal, followed by a promotional effect (Fig. 1a, b). Given that both Cys and phyllosilicates are likely involved in Cr(VI) reduction within the ternary reaction system, we compared the Cr(VI) removal amounts of the ternary system with the combined amounts of the two binary systems [i.e., Cys + Cr(VI) and biotite/chlorite + Cr(VI)] (Table S2). In the ternary system of Cys + biotite + Cr(VI), the Cr(VI) removal amounts were initially lower than the sum of the individual amounts from the biotite and Cys treatments at 3 days, but surpassed this sum after 4 days. A similar trend was observed in the ternary system of Cys + chlorite + Cr(VI). These results indicate a synergistic effect between Cys and biotite/chlorite in Cr(VI) removal. Cys is known to form complex with Fe(III) and cause the reduction of Fe(III) to Fe(II) (Doong and Schink, 2002; Hu et al., 2021; Morrison et al., 2013; Sheng et al., 2021), which may enhance the removal of Cr(VI).

The reduction of Cr(VI) by structure Fe(II) or aqueous Fe(II) occurs via three consecutive one-electron transfer steps, resulting in the rapid production and consumption of transient Cr(V) or Cr(IV) species (Joe-Wong et al., 2017; Liu et al., 2019). To directly detect the transient Cr(V) intermediate during Cr(VI) reduction, EPR analysis was conducted 77 K. As shown in Fig. 2, a distinct EPR signal with a *g*-value of ~1.98 was observed in both binary [that is, Cys + Cr(VI)] and ternary systems, indicating the formation of a solitary Cr(V) species (Chappell et al., 1998). Additionally, the Cr(V) signal intensity increased from 0 to 120 min in all systems, indicating the formation of relatively enduring Cr(V) complexes in the presence of Cys alone as well as in conjunction with phyllosilicates. These results suggested that following the reduction of Cr(VI) to Cr(V) in these reaction systems, the resulting Cr(V) species then forms complexes with Cys or its reaction products (such as cystine) (Bhattacharyya et al., 2013; Hu et al., 2021; Kieber et al., 2005), leading to the formation of relatively stable Cr(V) species that can be detected by EPR. Interestingly, the change Cr(V) signal intensity mirrored the trend in the rate of Cr(VI) reduction (Fig. 1). Specifically, during the initial 10 min, the Cr(V) signal intensity was weaker in the ternary groups compared to the binary group of Cys + Cr(VI). This suggests a competition between Cr(VI) and the phyllosilicates for reaction with Cys, indicating the diversion of electrons from Cys to structural Fe(III) in phyllosilicates. Subsequently, the Cr(V) signal intensity in the ternary system became significantly stronger than in the binary system, particularly in the presence of chlorite (Fig. 2c). This enhancement in the latter stages may be attributed to *in-situ* Fe(II) generated from Cys-induced reductive dissolution of the phyllosilicates, which initially reduces Cr(VI) to Cr(V), and then rapidly complexes with Cys or its oxidation products. Similar formation of Cr(V) complexes has been observed during Cr(VI) reduction by reduced nontronite in the presence of α-hydroxyl and carbonyl carboxylates (Liu et al., 2019). Thus, the results of Cr(VI) reduction kinetics and EPR suggested that the formation of *in-situ* Fe(II) was the underlying reason that the phyllosilicates provided additional electrons to promote Cr(VI) reduction by Cys under near-neutral pH conditions.

3.2. Reduced products of Cr(VI)

To determine whether the reduction product of Cr(VI) is soluble in the presence of both Cys and phyllosilicates, the concentration of total Cr in solution was measured over time (Fig. 1c, d). The results showed that initially, the total aqueous Cr concentration in the ternary groups exceeded the aqueous Cr(VI) concentration, and then gradually approached the Cr(VI) concentration (Fig. 1). This dynamic suggests that the initially formed soluble Cr(III) products underwent a gradual transformation into a solid phase, implying that the majority of the reduced Cr products were immobilized in the solid phase. Similar phenomena have been observed during the reduction of Cr(VI) by reduced nontronite in the presence of lactate (Liu et al., 2019). In contrast to the dominance of insoluble Cr(III)-organic complexes as observed in our study, previous studies observed that the presence of organic acids (e.g., tartrate and malate) resulted in a transformation of the reaction products from insoluble Cr(III) nanoparticles to soluble organic-complexed Cr(III) (Liu et al., 2018, 2019). This discrepancy may be attributed to the stronger affinity of Cys and its oxidation products for Fe-bearing phyllosilicates (Morrison et al., 2013; Sun et al., 2020), leading to the

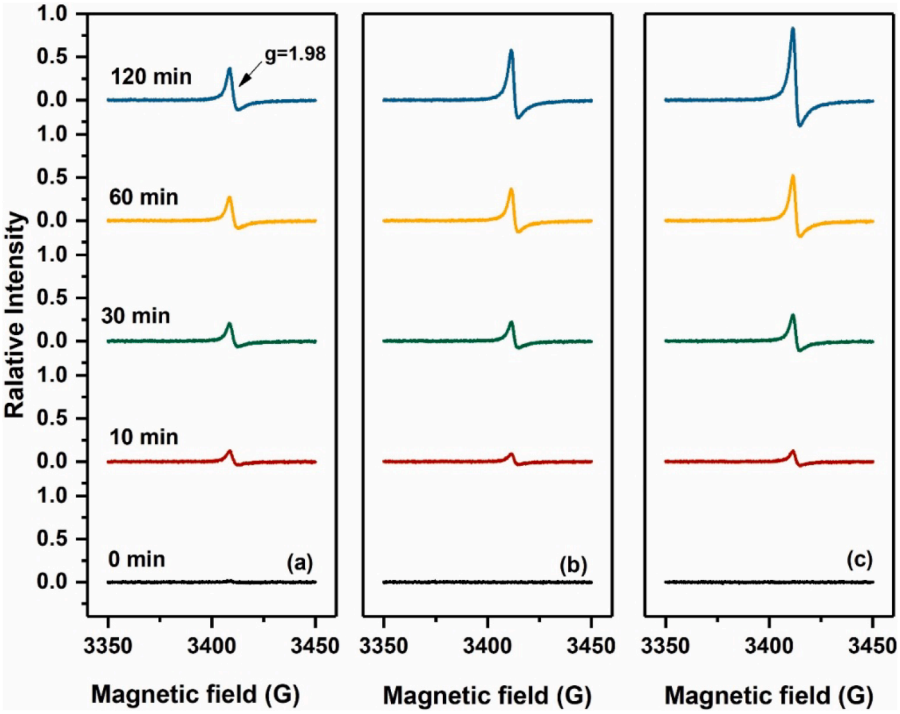

Fig. 2. EPR signal of the Cr(V) intermediate in the in the presence of (a) Cys, (b) Cys + Biotite, and (c) Cys + Chlorite at a pH of 6.0. Reaction conditions: 5.0 mM initial Cys, 5.0 mM initial aqueous Cr(VI), 5 $g \cdot L^{-1}$ biotite/chlorite, and 10 mM KBr (pH 6.0 was buffered with MES).

formation of stable Cr(III) complexes associated with phyllosilicates.

The Cr 2p XPS spectra revealed distinct peaks at Cr 2p3/2 ~576.8 eV and Cr 2p1/2 ~586.5 eV (Figure S3), indicating the exclusive presence of Cr(III) on the phyllosilicates surface (Liu et al., 2019; Wang et al., 2023; Xu et al., 2022). TEM images of the solid products displayed the presence of irregular aggregates on the edge of the minerals. Elemental mapping of these aggregates showed a clustering of Cr, S, and O, with a strong correlation between the Cr and S signals. Additionally, uniform Cr and S signals were observed on the mineral surface (Fig. 3). These XPS and TEM evidence, combined with the discrepancy between the concentrations of Cr(VI) and total Cr in solution (Fig. 1), suggest that most of the reduced Cr(VI) is present in solid form, likely as Cr(III)-organic complexes on the mineral surface. This implies that most of the Cr(VI) reduction products in the ternary group initially existed as soluble, organically complexed Cr(III), which was subsequently adsorbed onto the surface (Fig. 1). Similar dominant formation of Cr(III)-organic complexes were also observed during the reduction of Cr(VI) by aqueous Fe(II), zero-valent iron, or pyrite in the presence of organic ligands (Buerge and Hug, 1998; Kantar et al., 2015; Rivero-Huguet and Marshall, 2009). The combination of impermeable mineral matrix and insoluble Cr(III)-organic complex could potentially minimize Cr(III) re-oxidation and re-mobilization.

HR-TEM observations revealed the common presence of nanometer-sized Cr-containing particles on the edges of both biotite and chlorite (Figure S4), which are likely composed of Cr(III), possibly in the form of Cr_2O_3/$Cr(OH)_3$. Confirmation of this phase by XRD was unsuccessful (Figure S1a), likely due to its low abundance and sub-nanometer size. Nevertheless, the formation of Cr_2O_3/$Cr(OH)_3$ is consistent with previous studies that have identified nanometer-sized insoluble Cr_2O_3/$Cr(OH)_3$ particles as products of Cr(VI) reduction by structural Fe(II) in reduced clays (Bishop et al., 2014, 2019; Liu et al., 2018, 2019). Furthermore, TEM-EDS analysis revealed a typical composition of biotite/chlorite, with the presence of some Cr. Additionally, the TEM-EDS also indicated a co-occurrence of Fe and Cr, with markedly lower Cr and Fe signals detected in the bulk compared to those at the edge of biotite/chlorite (Fig. 3). The presence of Cr_2O_3/$Cr(OH)_3$ on the edges of phyllosilicates suggests a potential mechanism for Cr(VI) reduction, whereby negatively charged Cr(VI) is adsorbed onto the positively charged edges of phyllosilicates. Subsequently, reduction takes place through interfacial electron transfer involving edge-bound Fe(II), and/or through solid-state electron transfer involving structural Fe(II) within the phyllosilicates. The occurrence of multiple types of reduced Cr(III) suggested that various Cr(VI) reduction pathways and electron transfer processes occur within the ternary reaction system.

3.3. *Cys-induced phyllosilicates dissolution*

Cys possesses the capability of reducing structural Fe(III) within phyllosilicates (De Santana et al., 2010; Doong and Schink, 2002; Fang et al., 2023; Hu et al., 2021; Morrison et al., 2013; Sun et al., 2020). In this study, if Cys is able to induce the reduction and even dissolution of biotite/chlorite, it could lead to the release of Fe(II) and Fe(III) into the solution. This, on one hand, would promote interaction between the non-structural Fe(II) and Cr(VI). Numerous studies have demonstrated that Fe(II) bound to Fe-bearing mineral surfaces exhibits a markedly enhanced capacity of reducing oxidized contaminants compared to aqueous Fe(II) alone (Gorski and Scherer, 2009; Gregory et al., 2004; Pecher et al., 2002). Moreover, adsorbed Fe(II) can exchange Fe atoms

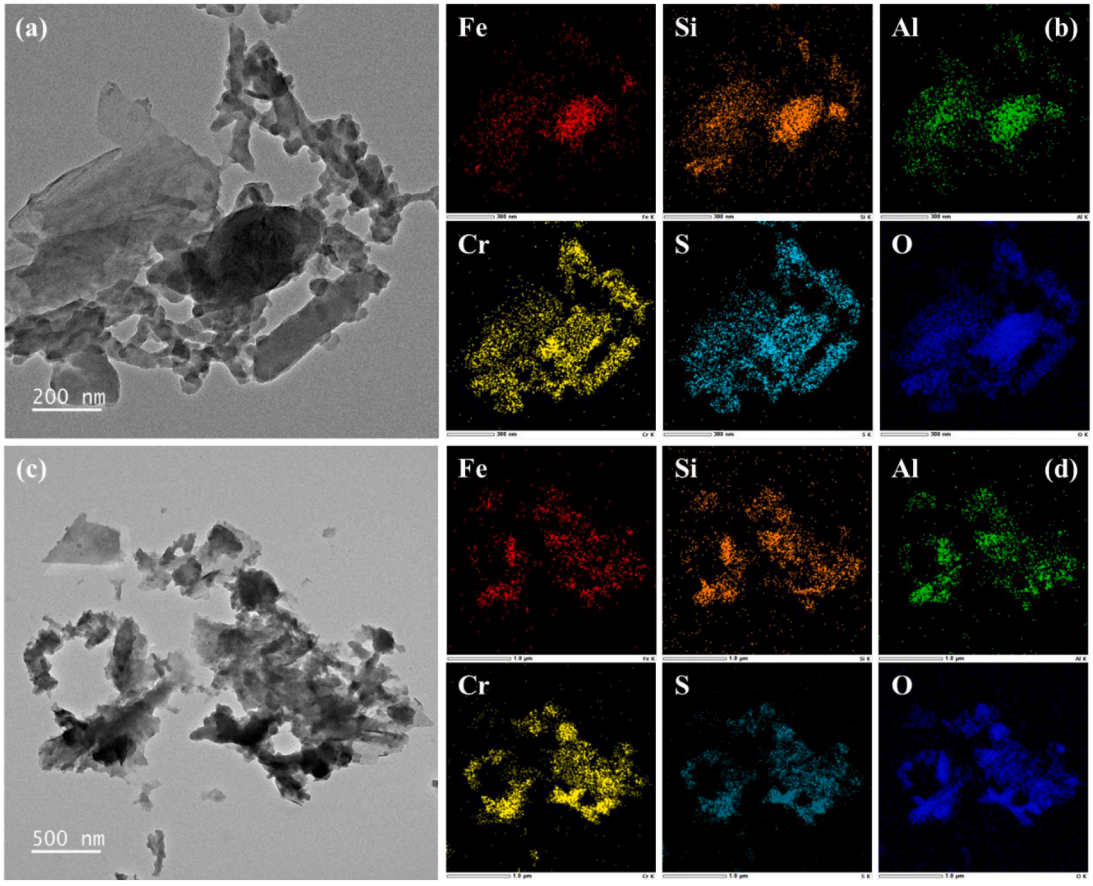

Fig. 3. (a) TEM image and (b) TEM-EDS mapping for the distribution of Fe, Si, Al, Cr, S, and O on solid products after 5 days of reaction in Cys + biotite + Cr(VI) group, (c) TEM image and (d) TEM-EDS mapping for the distribution of Fe, Si, Al, Cr, S, and O on solid products after 5 days of reaction in Cys + chlorite + Cr(VI) group. Reaction conditions: 0.5 mM initial Cys, 0.5 mM initial aqueous Cr(VI), 5 g·L $^{-1}$ biotite/chlorite, and 10 mM KBr (pH 6.0 was buffered with MES).

with structural Fe in Fe-bearing phyllosilicates (Latta et al., 2017; Neumann et al., 2013, 2015), so Fe(II) adsorbed on the surface of biotite/chlorite is highly likely to transfer electrons to structure Fe(III) of biotite/chlorite, resulting in the enhancing electron conduction and the Cr(VI) reduction. The reduction and dissolution of biotite/chlorite, on the other hand, would also stimulate the formation of soluble Cys-Fe(II) and/or Cys-Fe(III) complexes (Bhattacharyya et al., 2013; Fang et al., 2023; Zhou et al., 2023). The former complex exhibits a lower reducing potential compared to aqueous Fe(II), while the latter one has a catalytic effect on Cys electron donation (Gaberell et al., 2003; Hu et al., 2021; Liu et al., 2018). Both of these factors contribute to enhanced electron transfer from Cys or Fe(II) to Cr(VI), thereby accelerating Cr(VI) reduction.

To verify whether Cys can induce the dissolution of biotite/chlorite, a controlled experiment [i.e., Cys + biotite/chlorite] was conducted. Both biotite and chlorite are 2:1 phyllosilicate featuring an octahedrally coordinated layer of Mg and Fe ions sandwiched between sheets of linked SiO_4 tetrahedra (Brookshaw et al., 2014b). In this context, dissolved Si acts as an indicator of the dissolution rate of the tetrahedral layer, while dissolved Mg reflects the dissolution of the octahedral layer (Hopf et al., 2009). The results showed that a minimal quantity of Fe was released from phyllosilicates in the absence of Cys (Figure S5). However, in the presence of Cys, the percentage of released Fe from biotite and chlorite increased to 5.5 % and 7.8 %, respectively. Additionally, the Fe in the solution was predominantly Fe(II) (Figure S6). This suggests that the non-structural Fe(III), generated from mineral dissolution induced by Cys, continues to be reduced to Fe(II) by Cys in the solution. Similarly, the presence of Cys led to a notable increase in the release of Si and Mg (Figure S5). Dissolved Fe concentrations were an order of magnitude lower than the other elements, possibly due to the formation of green rust and $Fe(OH)_2$ (He et al., 2005). In the ternary system, dissolved Fe was also detected and was positively charged, making its complexation with negatively charged functional groups of cysteine or cystine theoretically plausible (Kieber et al., 2005). In this system, the Fe(II) and Fe (III) released during this reductive dissolution process may accelerate Cr (VI) reduction, by direct contact and/or by forming Cys-Fe(II/III) complexes to transfer electrons, as previously confirmed in systems involving clay minerals/soils, e.g., citric acid/soil, citric acid/reduced nontronite, and citric acid/montmorillonite (Kwak et al., 2017; Liu et al., 2018, 2019; Yang et al., 2008). In contrast to Morrison et al. (2013), which indicated that a ferruginous dioctahedral smectite (SWa-1) can be reduced by interlayer adsorption of Cys while the structure Fe remains fixed in the crystal lattice structure, our data revealed that Cys induced phyllosilicates dissolution. This discrepancy may be attributed to differences in the mineral's chemical structure, such as variations in interlayer spacing, expansibility, and Fe(III) content (Masson et al., 2024).

3.4. *Effect of mineral structure evolution on Cr(VI) reduction*

The structural evolution of the phyllosilicates and its effects on the Cr (VI) reduction was further considered. XRD confirmed the absence of secondary minerals in both binary and ternary systems (Figure S1a). While the phyllosilicates were found to be mineralogically pure, subtle changes in peak positions were observed. Specifically, after incubated with Cys, the *d*(001) spacing of biotite increased from 9.98 Å to 10.13 Å, and the *d*(003) spacing of chlorite increased from 7.07 Å to 7.11 Å (Figure S1b). Therefore, a certain quantity of Cys intercalated into the interlayers of both biotite and chlorite, agreeing with a previous study that observed Cys into the *d*(00*l*) interlayer spaces of SWa-1 (Morrison et al., 2013). The interlayer adsorption of Cys can facilitate a redox reaction involving a single electron exchange between the thiol functional group and the Fe(III) in the phyllosilicate structures (Morrison et al., 2013; Sun et al., 2020). The results also indicated the involvement of the interlayer region of these phyllosilicates in the electron transfer process. In the presence of Cr(VI) [that is, Cys + biotite/chlorite + Cr(VI)], the extent of increase in the interlayer spacing of both biotite and chlorite was decreased (Figure S1b). At a pH of ~ 6.0 applied in this study, the primary species of Cr(VI) and Cys were dominated by $HCrO_4^-/CrO_4^{2-}$ and H_2Cys^0 (Gennari et al., 2014), respectively, while biotite and chlorite are expected to be negatively charged (Luo et al., 2022). This allows Cys to adsorb onto and enter the structure of the phyllosilicates while simultaneously reducing Cr(VI). Previous literature using infrared spectroscopy has shown that Cys is adsorbed as a zwitterion on the surface of SWa-1 (Morrison et al., 2013). Consequently, the adsorption and/or intercalation of Cys to the phyllosilicates may impede the efficiency of electron transfer from Cys to Cr(VI), leading to a decrease in the rate of Cr(VI) reduction during the initial stage of the Cys + biotite/chlorite + Cr(VI) group (Fig. 1). Additionally, the consumption of Cys by Cr(VI) reduces the amount of Cys available to adsorb and/or enter the phyllosilicate structure (Figure S1).

The majority of the structural Fe(III) atoms within biotite and chlorite are situated in the octahedral layers [^{Oct}Fe(III)] (Brookshaw et al., 2014b; De Grave et al., 1987). The interactions between Cys and ^{Oct}Fe (III) were previously hypothesized to be linked to electron transfers from the tetrahedral surface to octahedral sites via ditrigonal cavities (Sun et al., 2020). According to previous studies, Cys not only intercalates into the phyllosilicate interlayers, but also reduces the structural Fe(III) (Morrison et al., 2013; Sun et al., 2020). ^{57}Fe Mössbauer spectroscopy was employed to determine the speciation and coordination environments of Fe within the bulk minerals (Fig. 4). Both biotite and chlorite exhibited a prominent doublet with a large quadrupole splitting, representing the Fe(II) contribution, as well a shoulder indicating a doublet at lower isomer shift attributable to the Fe(III) present. Based on the relative areas of the fitted doublets, the Fe(III) content accounted for approximately 25.3 % of the total Fe in biotite and 10.2 % in chlorite (refer to the Text S3 for further details on modeling parameters).

After 5 days incubated with Cys, the structure Fe(III) in both biotite and chlorite experienced a reduction of ~10 % (Fig. 4 and Table S3). The decrease in Fe(III) in biotite was accompanied by an increase of Fe(II) in the more abundant Fe-site, which according to the mineral structure is the *cis*-coordinated site (Brookshaw et al., 2014b). This indicates that the conversion of Fe(III) to Fe(II) primarily takes place at the *cis*-coordinated sites within the bulk of the mineral. The slight variation in the relative abundance of Fe(II) at the *trans*-coordinated sites could be attributed to the preoccupation of most of these sites by Fe(II) (Brookshaw et al., 2015), which is also supported by theoretical calculations suggesting that the *trans*-coordinated sites may function as electron traps (Rosso and Ilton, 2003). A similar phenomenon also occurred in chlorite structures (Fig. 4 and Table S3). Mössbauer spectroscopy characterizes the solid-state Fe speciation and is not sensitive to sorbed Fe speciation at room temperature. Therefore, these results demonstrate that Cys was able to reduce a substantial fraction of the structural Fe(III) in biotite and chlorite. The relative changes in bulk Fe speciation in the present study were similar to those observed during microbially mediated Fe(III) reduction (Brookshaw et al., 2014a, b). Consequently, a large proportion of structural Fe(III) in biotite and chlorite may be susceptible to *in-situ* conversion to Fe(II) by a range of coexisting constituents in the environment.

In the presence of Cr(VI) [that is, Cys + biotite/chlorite + Cr(VI)], the fraction of *cis*-coordinated Fe(II) in biotite decreased to 47.5 %, while the fraction of *trans*-coordinated Fe(II) increased to 27.9 % (Fig. 4 and Table S3). Therefore, the oxidation of Fe(II) preferentially occurred at the *cis*-coordinated octahedral sites upon Cr(VI) reduction. The fact that *cis*-octahedral sites oxidize more readily than *trans* sites is consistent with the relatively small size of the former sites (given that Fe(III) is a markedly smaller ion than Fe(II)) and with the proposed *cis*-site occupation of the intrinsic Fe(III) in mica and related minerals (Rancourt et al., 1993). This implies that *cis*-coordinated Fe(II) in biotite exhibits higher activity in electron donation and participation in Cr(VI) reduction compared to *trans*-coordinated Fe(II). Similarly, the fraction of *cis*-coordinated Fe(II) in chlorite decreased from 43.9 % to 42.7 %, while

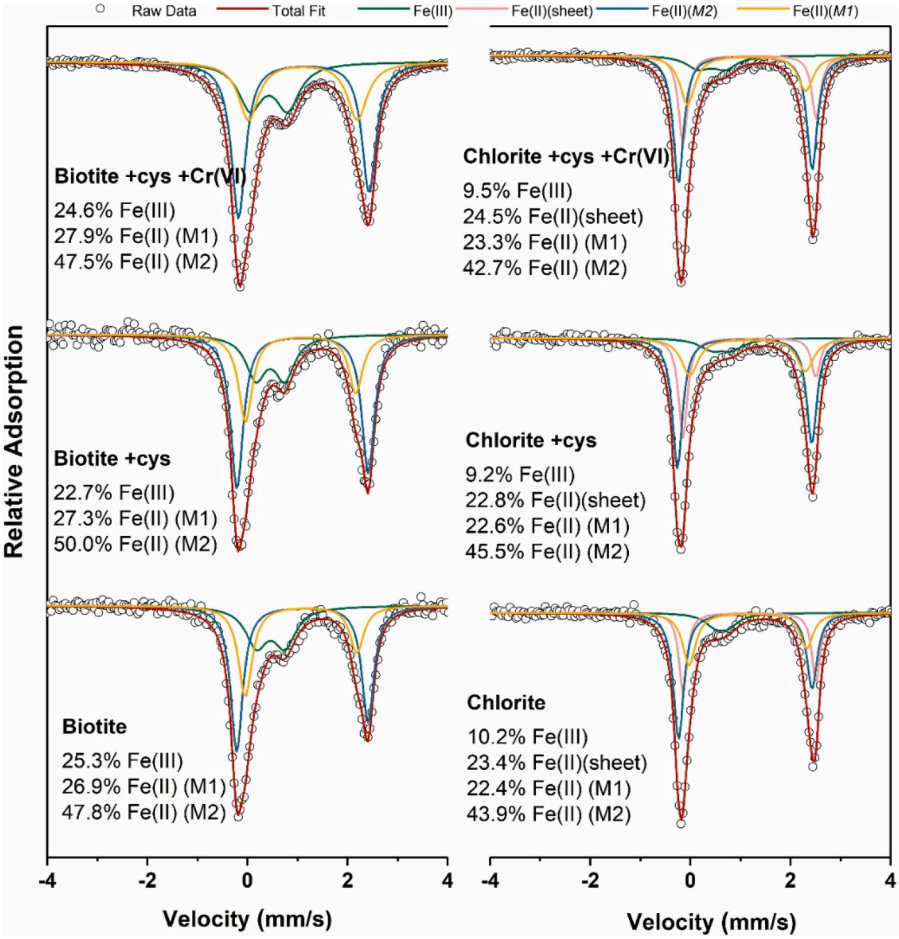

Fig. 4. Mössbauer spectra of Fe in pristine and reacted samples of biotite and chlorite from the Cys + biotite/chlorite and Cys + biotite/chlorite + Cr(VI) groups after 5 days of reaction. Reaction conditions: 0.5 mM initial Cys, 0.5 mM initial aqueous Cr(VI), 5 g·L^{-1} biotite/ chlorite, and 10 mM KBr (pH 6.0 was buffered with MES). M1 and M2 refer to the *trans*-coordinated site and *cis*-coordinated site of Fe(II) in the phyllosilicate's octahedral layer, respectively. Sheet refers to Fe(II) in the brucite-like interlayer of chlorite.

the fraction of *trans*-coordinated Fe(II) and brucite structure increased by 4.0 % and 4.7 %, respectively (Fig. 4 and Table S3). This suggests that *cis*-coordinated Fe(II) in chlorite demonstrate the most favorable characteristics for electron donation and participation in Cr(VI) reduction, while *trans*-coordinated Fe(II) exhibits the least favorable behavior. The reactivity disparities among different Fe(II) entities within the phyllosilicate structure have been observed for organic compounds, Tc(VII), and U(VI) (Bishop et al., 2011; Chen et al., 2019; Zhang et al., 2011). Together with these spectroscopic evidence, our results indicate that, apart from Cys and non-structural Fe(II), structural Fe(II) present in biotite/chlorite is also involved in the reduction of Cr(VI).

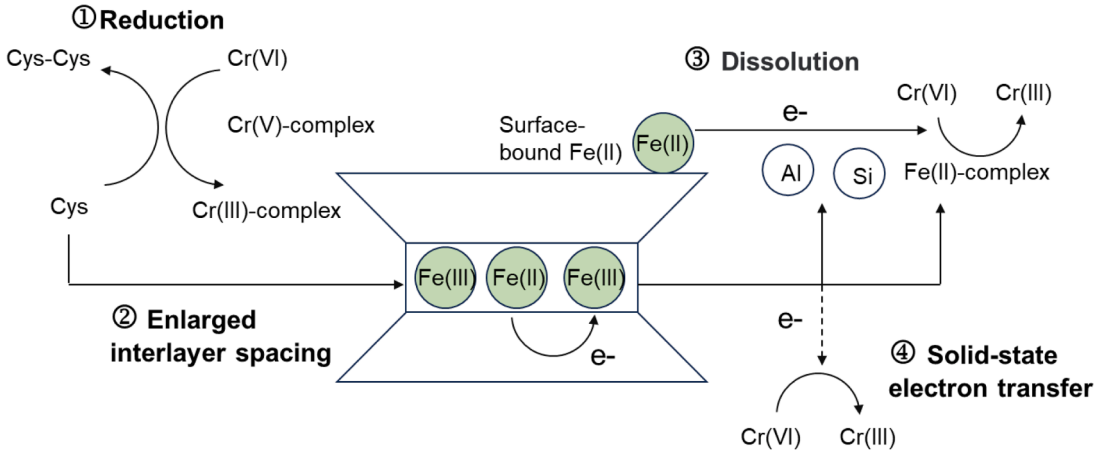

Fig. 5. Proposed reaction mechanism for synergistic Cr(VI) reduction by structural Fe(II) in phyllosilicates and organic ligands under near-neutral pH conditions.

3.5. Mechanisms of Cr(VI) reduction in the presence of CYS and phyllosilicates

Based on the aforementioned evidence, four interrelated mechanisms are proposed to collectively influence the kinetics of Cr(VI) removal in the presence of Cys-phyllosilicates (Fig. 5). (i) Cys directly reduces Cr(VI) through a successive three-step electron transfer process in the aqueous phase, during which the transient Cr(V) intermediate is formed. This process serves as the primary mechanism of Cr(VI) reduction in the initial stage of the reaction. (ii) The phyllosilicate competes with Cr(VI) for reaction with Cys, wherein Cys infiltrates the phyllosilicate structure, resulting in an expansion of the interlayer spacing. The intercalation of Cys into these interlayer spaces facilitates electron exchange, potentially occurring through the ditrigonal cavities in the tetrahedral sheets. This electron exchange process subsequently brings about the reduction of structural Fe(III) to Fe(II) within the mineral structure. (iii) Cys induces phyllosilicates dissolution, leading the release of Fe(II) into the solution. Subsequently, these non-structural Fe(II) species form Cys-Fe(II) complexes and phyllosilicate surface bound Fe(II), which contribute to the reduction of Cr(VI). (iv) The octahedral Fe(II) within the mineral engages in solid-state electron transfer, reducing the adsorbed Cr(VI) at the edges of the phyllosilicates. Overall, the reduction of Cr(VI) observed in this study is a distinctive outcome of the interplay between Cys and phyllosilicates, characterized by an initial inhibitory effect followed by a promoting effect. Cys plays a dual role as both organic ligands and electron donors in this process.

4. Conclusions

In-situ produced Fe(II) from microbial or abiotic reduction of structural Fe(III) in phyllosilicates plays an important role in the fate and transport of contaminants in natural environments. This work investigated the interfacial reduction processes of Cr(VI) on Fe(II/III)-bearing phyllosilicates (biotite and chlorite) induced by Cys, emphasizing the importance of abiotic Fe(III) reduction in contaminant dynamics. Based on the results, the following key conclusions can be drawn:

- The presence of Cys markedly enhances the reactivity of biotite and chlorite towards Cr(VI) reduction, achieving this reduction through a single electron transfer process and the formation of Cr(V) intermediates.
- Cys functions as both an organic ligand and an electron donor in Cr (VI) reduction. It is capable of self-reducing Cr(VI) and inducing the reduction and dissolution of phyllosilicates to generate *in-situ* Fe(II), which further participates in Cr(VI) reduction. Additionally, Cys can form complexes with the reduction products of Cr(VI).
- Fe(II) with different entities in both biotite and chlorite exhibit varying levels of activity in electron donation and participation in Cr (VI) reduction, highlighting the significance of structural Fe(II) coordination in phyllosilicates on the reactivity towards contaminants.
- The reduction products of Cr(VI) mainly exist in the form of insoluble Cr(III)-organic complex and sub-nanometer Cr_2O_3/$Cr(OH)_3$, associated with residual minerals as micro-aggregates. This textural association was expected to minimize the chance of Cr(III) reoxidation upon exposure to oxidants.
- The results suggested that electron-shuttling compounds like Cys can induce structural evolution in Fe-bearing phyllosilicates, which may significantly influence or control the long-term migration and transformation of reducible pollutants in aquatic and terrestrial ecosystems. This study provides mechanistic insights into the interfacial electron transfer processes of redox-active pollutants on Fe-bearing phyllosilicates and has substantial implications for the development of long-term, *in-situ* immobilization technologies for pollutant remediation.

CRediT authorship contribution statement

Fei Wu: Writing – original draft, Methodology, Investigation, Funding acquisition, Conceptualization. **Jing Sun:** Writing – review & editing. **Fangyuan Meng:** Formal analysis. **Jimei Zhou:** Writing – review & editing. **Meng Qi:** Formal analysis. **Xiaoli Lu:** Formal analysis. **Chengshuai Liu:** Writing – review & editing, Supervision, Project administration, Funding acquisition.

Declaration of competing interest

The authors declare that they have no known competing financial interests or personal relationships that could have appeared to influence the work reported in this paper.

Data availability

Data will be made available on request.

Acknowledgements

This work was financially supported by the National Natural Science Foundations of China (42025705 and 42207314), the China Postdoctoral Science Foundation (2022M713125), and Guizhou Province High-level Talent Project (GCC [2022]002-1).

Supplementary materials

Supplementary material associated with this article can be found, in the online version, at doi:10.1016/j.watres.2024.122548.

References

Bhattacharyya, A., Stavitski, E., Dvorak, J., Martínez, C.E., 2013. Redox interactions between Fe and Cysteine: spectroscopic studies and multiplet calculations. Geochim. Cosmochim. Acta 122, 89–100.
Bishop, M.E., Dong, H., Glasser, P., Briggs, B.R., Pentrak, M., Stucki, J.W., Boyanov, M.I., Kemner, K.M., Kovarik, L., 2019. Reactivity of redox cycled fe-bearing subsurface sediments towards hexavalent chromium reduction. Geochim. Cosmochim. Acta 252, 88–106.
Bishop, M.E., Dong, H., Kukkadapu, R.K., Liu, C., Edelmann, R.E., 2011. Bioreduction of Fe-bearing clay minerals and their reactivity toward pertechnetate (Tc-99). Geochim. Cosmochim. Acta 75 (18), 5229–5246.
Bishop, M.E., Glasser, P., Dong, H., Arey, B., Kovarik, L., 2014. Reduction and immobilization of hexavalent chromium by microbially reduced Fe-bearing clay minerals. Geochim. Cosmochim. Acta 133, 186–203.
Bohrer, D., Bortoluzzi, F., Nascimento, P.C., Carvalho, L.M., Ramirez, A.G., 2008. Silicate release from glass for pharmaceutical preparations. Int. J. Pharm. 355 (1–2), 174–183.
Brookshaw, D.R., Coker, V.S., Lloyd, J.R., Vaughan, D.J., Pattrick, R.A., 2014a. Redox interactions between Cr(VI) and Fe(II) in bioreduced biotite and chlorite. Environ. Sci. Technol. 48 (19), 11337–11342.
Brookshaw, D.R., Lloyd, J.R., Vaughan, D.J., Pattrick, R.A.D., 2014b. Bioreduction of biotite and chlorite by a shewanella species. Am. Mineral 99 (8–9), 1746–1754.
Brookshaw, D.R., Pattrick, R.A.D., Bots, P., Law, G.T.W., Lloyd, J.R., Mosselmans, J.F.W., Vaughan, D.J., Dardenne, K., Morris, K., 2015. Redox interactions of Tc(VII), U(VI), and Np(V) with microbially reduced biotite and chlorite. Environ. Sci. Technol. 49 (22), 13139–13148.
Buerge, I.J., Hug, S.J., 1998. Influence of organic ligands on chromium(VI) reduction by iron(II). Environ. Sci. Technol. 32 (14), 2092–2099.
Cakir, S., Bicer, E., 2005. The interaction of cysteine with chromium(VI) ions under UV irradiation. Bioelectrochemistry 67 (1), 75–80.
Chappell, J., Chiswell, B., Canning, A., 1998. Quantitative analysis of chromium(V) by EPR spectroscopy. Talanta 46 (1), 23–38.
Chen, N., Huang, M., Liu, C., Fang, G., Liu, G., Sun, Z., Zhou, D., Gao, J., Gu, C., 2019. Transformation of tetracyclines induced by Fe(III)-bearing smectite clays under anoxic dark conditions. Water Res. 165, 114997.
De Grave, E., Vandenbruwaene, J., Van Bockstael, M., 1987. ^{57}Fe Mössbauer spectroscopic analysis of chlorite. Phys. Chem. Minerals 15, 173–180.
Deng, L., Liu, F., Ding, Z., Liang, Y., Shi, Z., 2023. Effect of natural organic matter on Cr (VI) reduction by reduced nontronite. Chem. Geol. 615, 121198.
De Santana, H., Paesano Jr., A., da Costa, A.C., di Mauro, E., de Souza, I.G., Ivashita, F.F., de Souza, C.M., Zaia, C.T., Zaia, D.A., 2010. Cysteine, thiourea and thiocyanate interactions with clays: FT-IR, mössbauer and EPR spectroscopy and X-Ray diffractometry studies. Amino Acids 38 (4), 1089–1099.

Dong, H., 2012. Clay-Microbe interactions and implications for environmental mitigation. Elements 8 (2), 113–118.
Doong, R.A., Schink, B., 2002. Cysteine-Mediated reductive dissolution of poorly crystalline Iron(III) oxides by geobacter sulfurreducens. Environ. Sci. Technol. 36 (13), 2939–2945.
Fan, Q., Wang, L., Fu, Y., Li, Q., Liu, Y., Wang, Z., Zhu, H., 2023. Iron redox cycling in layered clay minerals and its impact on contaminant dynamics: a review. Sci. Total Environ. 855, 159003.
Fang, L., Chi, J., Shi, Q., Wu, Y., Li, F., 2023. Facet-Dependent electron transfer induces distinct arsenic reallocations on hematite. Water Res. 242, 120180.
Favre, F., Stucki, J.W., Boivin, P., 2006. Redox properties of structural Fe in ferruginous smectite. A discussion of the standard potential and its environmental implications. Clays Clay Miner. 54 (4), 466–472.
Gaberell, M., Chin, Y.P., Hug, S.J., Sulzberger, B., 2003. Role of dissolved organic matter composition on the photoreduction of Cr(VI) to Cr(III) in the presence of iron. Environ. Sci. Technol. 37 (19), 4403–4409.
Gennari, F., Sharma, V.K., Pettine, M., Campanella, L., Millero, F.J., 2014. Reduction of selenite by cysteine in ionic media. Geochim. Cosmochim. Acta 124, 98–108.
Gorski, C.A., Scherer, M.M., 2009. Influence of magnetite stoichiometry on Fe(II) uptake and nitrobenzene reduction. Environ. Sci. Technol. 43 (10), 3675–3680.
Gregory, K.B., Larese-Casanova, P., Parkin, G.F., Scherer, M.M., 2004. Abiotic transformation of hexahydro-1,3,5-trinitro-1,3,5-triazine by Fe^{II} bound to magnetite. Environ. Sci. Technol. 38 (5), 1408–1414.
He, Y.T., Bigham, J.M., Traina, S.J., 2005. Biotite dissolution and Cr(VI) reduction at elevated pH and ionic strength. Geochim. Cosmochim. Acta 69 (15), 3791–3800.
Hopf, J., Langenhorst, F., Pollok, K., Merten, D., Kothe, E., 2009. Influence of microorganisms on biotite dissolution: an experimental approach. Geochemistry 69, 45–56.
Hu, S., Liu, T., Yang, Y., Li, F., Fang, L., 2021. Cysteine induced cascade electron transfer by forming a unique ternary complex with Fe(II) on goethite. Chem. Geol. 584, 120561.
Huang, J., Jones, A., Waite, T.D., Chen, Y., Huang, X., Rosso, K.M., Kappler, A., Mansor, M., Tratnyek, P.G., Zhang, H., 2021. Fe (II) redox chemistry in the environment. Chem. Rev. 121 (13), 8161–8233.
Jaisi, D.P., Dong, H., Plymale, A.E., Fredrickson, J.K., Zachara, J.M., Heald, S., Liu, C., 2009. Reduction and long-term immobilization of technetium by Fe(II) associated with clay mineral nontronite. Chem Geo 264 (1–4), 127–138.
Jocelyn, P.C., 1967. The standard redox potential of cysteine-cystine from the thiol-disulphide exchange reaction with glutathione and lipoic acid. Eur. J. Biochem. 2 (3), 327–331.
Joe-Wong, C., Brown Jr., G.E., Maher, K., 2017. Kinetics and products of chromium(VI) reduction by iron(II/III)-bearing clay minerals. Environ. Sci. Technol. 51 (17), 9817–9825.
Kantar, C., Ari, C., Keskin, S., 2015. Comparison of different chelating agents to enhance reductive Cr(VI) removal by pyrite treatment procedure. Water Res. 76, 66–75.
Kieber, R.J., Skrabal, S.A., Smith, B.J., Willey, J.D., 2005. Organic complexation of Fe(II) and its impact on the redox cycling of iron in rain. Environ. Sci. Technol. 39 (6), 1576–1583.
Kim, H.-B., Kim, J.-G., Kim, S.-H., Kwon, E.E., Baek, K., 2019. Consecutive reduction of Cr(VI) by Fe(II) formed through photo-reaction of iron-dissolved organic matter originated from biochar. Environ. Pollut. 253, 231–238.
Kwak, S., Yoo, J.-C., Baek, K., 2017. Synergistic and inhibitory reduction of Cr(VI) by montmorillonite, citric acid, and Mn(II). J. Soils Sediments 18 (1), 205–210.
Latta, D.E., Neumann, A., Premaratne, W.A.P.J., Scherer, M.M., 2017. Fe(II)-Fe(III) electron transfer in a clay mineral with low Fe content. ACS Earth Space Chem. 1 (4), 197–208.
Lay, P.A., Levina, A., 1996. Kinetics and mechanism of chromium(VI) reduction to chromium(III) by L-cysteine in neutral aqueous solutions. Inorg. Chem 35 (26), 7709–7717.
Li, J., Shi, C., Zeng, W., Wang, Y., Hong, Z., Ma, Y., Fang, L., 2022. Distinct roles of pH and organic ligands in the dissolution of goethite by cysteine. J. Environ. Sci. 113, 260–268.
Liao, P., Pan, C., Ding, W., Li, W., Yuan, S., Fortner, J.D., Giammar, D.E., 2020. Formation and transport of Cr(III)-NOM-Fe colloids upon reaction of Cr(VI) with NOM-Fe(II) colloids at anoxic-oxic interfaces. Environ. Sci. Technol. 54 (7), 4256–4266.
Liao, W., Ye, Z., Yuan, S., Cai, Q., Tong, M., Qian, A., Cheng, D., 2019. Effect of coexisting Fe(III) (oxyhydr)oxides on Cr(VI) reduction by Fe(II)-bearing clay minerals. Environ. Sci. Technol. 53 (23), 13767–13775.
Liu, K., Li, F., Pang, Y., Fang, L., Hocking, R., 2022. Electron shuttle-induced oxidative transformation of arsenite on the surface of goethite and underlying mechanisms. J. Hazard. Mater. 425, 127780.
Liu, X., Dong, H., Yang, X., Kovarik, L., Chen, Y., Zeng, Q., 2018. Effects of citrate on hexavalent chromium reduction by structural Fe(II) in nontronite. J. Hazard. Mater. 343, 245–254.
Liu, X., Dong, H., Zeng, Q., Yang, X., Zhang, D., 2019. Synergistic effects of reduced nontronite and organic ligands on Cr(VI) reduction. Environ. Sci. Technol. 53 (23), 13732–13741.
Liu, Y., Shi, S., Zeng, Q., Li, Y., Chen, Y., Guo, D., Hu, D., Dong, H., 2023. Coupled reduction of structural Fe(III) in nontronite and oxidation of petroleum hydrocarbons. Geochim. Cosmochim. Acta 344, 103–121.
Luan, F., Liu, Y., Griffin, A.M., Gorski, C.A., Burgos, W.D., 2015. Iron(III)-bearing clay minerals enhance bioreduction of nitrobenzene by shewanella putrefaciens CN32. Environ. Sci. Technol. 49 (3), 1418–1426.
Luo, D., Geng, R., Zhang, Y., Li, P., Liang, J., Fan, Q., Qiang, S., 2022. Interaction behaviors of Cr(VI) at biotite-water interface in the presence of HA: batch, XRD and XPS investigations. Chemosphere 293, 133585.
Masson, D., Robin, V., Joussein, E., Tertre, E., Baron, F., 2024. Role of the crystal chemistry on the dissolution kinetics of Fe(III)-rich smectites. Geochim. Cosmochim. Acta 371, 162–172.
Morrison, K.D., Bristow, T.F., Kennedy, M.J., 2013. The reduction of structural iron in ferruginous smectite via the amino acid cysteine: implications for an electron shuttling compound. Geochim. Cosmochim. Acta 106, 152–163.
Neumann, A., Olson, T.L., Scherer, M.M., 2013. Spectroscopic evidence for Fe(II)-Fe(III) electron transfer at clay mineral edge and basal sites. Environ. Sci. Technol. 47 (13), 6969–6977.
Neumann, A., Wu, L., Li, W., Beard, B.L., Johnson, C.M., Rosso, K.M., Frierdich, A.J., Scherer, M.M., 2015. Atom exchange between aqueous Fe(II) and structural Fe in clay minerals. Environ. Sci. Technol. 49 (5), 2786–2795.
Pecher, K., Haderlein, S.B., Schwarzenbach, R.P., 2002. Reduction of polyhalogenated methanes by surface-bound Fe(II) in aqueous suspensions of iron oxides. Environ. Sci. Technol. 36 (8), 1734–1741.
Rancourt, D.G., Tume, P., Lalonde, A.E., 1993. Kinetics of the $(Fe^{2+} + OH^{-})_{mica} \rightarrow (Fe^{3+} + O^{2-})_{mica} + H$ oxidation reaction in bulk single-crystal biotite studied by mössbauer spectroscopy. Phys. Chem. Minerals 20 (4), 276–284.
Rivero-Huguet, M., Marshall, W.D., 2009. Influence of various organic molecules on the reduction of hexavalent chromium mediated by zero-valent iron. Chemosphere 76 (9), 1240–1248.
Rosso, K.M., Ilton, E.S., 2003. Charge transport in micas: the kinetics of $Fe^{II/III}$ electron transfer in the octahedral sheet. J. Chem. Phys. 119 (17), 9207–9218.
Satpathy, A., Catalano, J.G., Giammar, D.E., 2022. Reduction of U(VI) on chemically reduced montmorillonite and surface complexation modeling of adsorbed U(IV). Environ. Sci. Technol. 56 (7), 4111–4120.
Sheng, Y., Dong, H., Kukkadapu, R.K., Ni, S., Zeng, Q., Hu, J., Coffin, E., Zhao, S., Sommer, A.J., McCarrick, R.M., Lorigan, G.A., 2021. Lignin-Enhanced reduction of structural Fe(III) in nontronite: dual roles of lignin as electron shuttle and donor. Geochim. Cosmochim. Acta 307, 1–21.
Slessarev, E.W., Lin, Y., Bingham, N.L., Johnson, J.E., Dai, Y., Schimel, J.P., Chadwick, O. A., 2016. Water balance creates a threshold in soil pH at the global scale. Nature 540 (7634), 567–569.
Sun, Z., Huang, M., Liu, C., Fang, G., Chen, N., Zhou, D., Gao, J., 2020. The formation of *OH with Fe-bearing smectite clays and low-molecular-weight thiols: implication of As(III) removal. Water Res. 174, 115631.
Wang, W., Shi, L., Wu, H., Ding, Z., Liang, J., Li, P., Fan, Q., 2023. Interactions between micaceous minerals weathering and cesium adsorption. Water Res. 238, 119918.
Wang, Y., Chen, S.-Y., Yang, X., Wu, Y., Huang, X.-F., He, E.-K., Qiu, R.-L., Wang, S., 2019. Enhanced removal of Cr(VI) in the Fe(III)/natural polyphenols system: role of the in situ generated Fe(II). J. Hazard. Mater. 377, 321–329.
Wielinga, B., Mizuba, M.M., Hansel, C.M., Fendorf, S., 2001. Iron promoted reduction of chromate by dissimilatory iron-reducing bacteria. Environ. Sci. Technol. 35 (3), 522–527.
Xu, Z., Yu, Y., Xu, X., Tsang, D.C.W., Yao, C., Fan, J., Zhao, L., Qiu, H., Cao, X., 2022. Direct and indirect electron transfer routes of Chromium(VI) reduction with different crystalline ferric oxyhydroxides in the presence of pyrogenic carbon. Environ. Sci. Technol. 56 (3), 1724–1735.
Yang, J.W., Tang, Z.S., Guo, R.F., Chen, S.Q., 2008. Soil surface catalysis of Cr(VI) reduction by citric acid. Environ. Prog. 27 (3), 302–307.
Zhang, D., Liu, X., Guo, D., Li, G., Qu, J., Dong, H., 2022. Cr(VI) reduction by siderophore alone and in combination with reduced clay minerals. Environ. Sci. Technol. 56 (17), 12315–12324.
Zhang, G., Burgos, W.D., Senko, J.M., Bishop, M.E., Dong, H., Boyanov, M.I., Kemner, K. M., 2011. Microbial reduction of chlorite and uranium followed by air oxidation. Chem. Geol. 283 (3–4), 242–250.
Zhang, L., Chen, Y., Xia, Q., Kemner, K.M., Shen, Y., O'Loughlin, E.J., Pan, Z., Wang, Q., Huang, Y., Dong, H., Boyanov, M.I., 2021. Combined effects of Fe(III)-bearing clay minerals and organic ligands on U(VI) bioreduction and U(IV) speciation. Environ. Sci. Technol. 55 (9), 5929–5938.
Zhang, L., Jun, Y.S., 2018. The role of Fe-bearing phyllosilicates in DTPMP degradation under high-temperature and high-pressure conditions. Environ. Sci. Technol. 52 (16), 9522–9530.
Zhou, F., Liu, Q., Qin, Y., Liu, W., Zhang, L., 2023. Efficient Fe(III)/Fe(II) cycling mediated by L-cysteine functionalized zero-valent iron for enhancing Cr(VI) removal. J. Hazard. Mater. 456, 131717.
Zhou, W., Xian, D., Su, X., Li, Y., Que, W., Shi, Y., Wang, J., Liu, C., 2020. Macroscopic and spectroscopic characterization of U(VI) sorption on biotite. Chemosphere 255, 126942.